Structure and Electronic Properties of Potassium-Loaded Zeolite L

P. A. Anderson,[†] A. R. Armstrong,[‡] A. Porch,[§] P. P. Edwards,*[,†] and L. J. Woodall[†]

School of Chemistry, The University of Birmingham, Edgbaston, Birmingham, B15 2TT, UK; School of Chemistry, The University, St. Andrews, Fife, KY16 9ST, UK; and School of Electronic and Electrical Engineering, The University of Birmingham, Edgbaston, Birmingham, B15 2TT

Received: May 29, 1997[⊗]

The structure, electron spin resonance, and electrical properties of potassium-loaded zeolite L have been studied as a function of metal loading up to a concentration of nine additional potassium atoms per unit cell. The incorporation of extra potassium into the dehydrated zeolite resulted in an increase in the room-temperature conductivity by a factor of 10 000 at the highest loading level. The strong temperature dependence of the measured electrical conductivities indicates that the conduction process is thermally activated throughout the composition range investigated. In accordance with theoretical predictions by M. J. Kelly, our measurements indicate that any anisotropy in the conductivity must be relatively modest. The role in the conduction mechanism of new K_3^{p+} clusters located in the one-dimensional channels is discussed.

Introduction

The regular intracrystalline channels and cavities of a dehydrated zeolite constitute a periodic array of cation-lined nanoscale spaces in which discrete chemical species—or alternatively, tiny fragments of bulk materials—may be assembled and arranged with a well-defined geometry relative to one other.[1] One advantage often sought by following this synthetic approach is an enhancement in either the stability or the desired properties of the "guest" component through encapsulation within the aluminosilicate framework of the host zeolite. In contrast, alkali metal loaded zeolites exhibit a qualitatively different form of host−guest interaction. This interaction is sufficiently strong to result in the spontaneous ionization of the incoming guest metal atoms to form a wide range of inclusion compounds whose properties bear little resemblance if any to those of the parent alkali metals.[2,3] The ionization of incoming alkali metal atoms by the intense electric fields within the zeolite facilitates the controlled release of "excess" electrons to interact with the zeolite cations, while the newly formed cations find sites coordinated to the zeolite framework. The phenomenon of alkali metal inclusion has been likened to the "dissolution" of alkali metals in the solid zeolite solvent.[3] This unique opportunity to control continuously and precisely the excess electron density over a wide range—within tightly confined dimensions, and without any significant structural change in the framework—has placed alkali metal loaded zeolites at the forefront of current research into materials design.[4]

The excess electrons released through the ionization of alkali metal atoms within the zeolite pores may be localized in well-defined traps. Electron spin resonance (ESR) studies have identified the occurrence of a range of colored paramagnetic centers of the form $K_m^{(m-1)+}$ and $Na_n^{(n-1)+}$ ($m = 3, 4$; $n = 3, 4, 5, 6$) in zeolites X, Y, A.[5−10] Although much of the work published to date on these systems has been directed toward the preparation and characterization of these paramagnetic centers or "clusters", in recent years the possibility of inducing electron delocalization throughout the entire zeolite structure has assumed particular significance.[2,3,11] This is a particularly attractive proposition in the case of zeolites whose natural structure consists of "infinite" one-dimensional channels as it raises the possibility of electron delocalization along a single crystallographic direction.[12]

In this regard, Kelly[4,13] has highlighted the poor prospects for practical quasi-one-dimensional electronic devices emerging from existing fabrication technologies, and identified metal loaded zeolites and related materials as offering one of the most promising routes toward this goal in the medium to long term. Zeolite L, with unit cell formula $K_9Al_9Si_{27}O_{72}$ (hereafter K_9-L), is an example of a potential host system, which contains 12-ring channels parallel to the *c* direction. We have previously reported[12] the results of a combined structural and ESR study of potassium zeolite L containing a single extra potassium per unit cell (K_1/K_9-L); this work highlighted the possibility of electron delocalization within the one-dimensional channels of the zeolite host. Here we present the results of a study of the structural, ESR, and electrical properties of the potassium-loaded potassium zeolite L system up to a metal loading of nine additional potassiums per unit cell (K_9/K_9-L).

Experimental Section

Sample Preparation. The compounds K_u/K_9-L were prepared through the reaction of dehydrated potassium zeolite LTL (K_9-L), supplied by Laporte, with an amount of potassium vapor equivalent to an extra *u* potassium atoms per zeolite unit cell. A range of samples with $u = 1, 3, 5, 7$, and 9 was chosen for initial study. After comprehensive measurements on this series, two further samples ($u = 2$ and 4) were prepared to provide some additional information. All the reactions were carried out in sealed, evacuated quartz reaction tubes, as described previously.[2] A suitable quantity of zeolite (typically 1−2 g) was placed in a reaction tube and evacuated overnight at 450 °C to better than 10^{-5} mbar. The reaction tube was then transferred to an argon drybox where potassium metal (Aldrich 99.95%), previously distilled into calibrated capillary tubes,[2] was introduced and returned to the vacuum line to be evacuated and sealed with a gas−oxygen torch. At no stage did the metal or sample come into contact with the atmosphere. On heating the sealed tube, potassium vapor filled the reaction chamber and spontaneous coloration of the zeolite occurred. Careful anneal-

* To whom correspondence should be addressed.
[†] School of Chemistry, Birmingham.
[‡] School of Chemistry, St. Andrews.
[§] School of Electronic and Electrical Engineering.
[⊗] Abstract published in *Advance ACS Abstracts,* October 15, 1997.

S1089-5647(97)01737-9 CCC: $14.00

ing at 200 °C for up to 66 h resulted in homogeneous blue solids of progressively darker shade with increasing amount of added metal.

Neutron Powder Diffraction. Time-of-flight neutron powder diffraction measurements were performed at room temperature on Polaris, the high-intensity, medium-resolution powder diffractometer at the ISIS pulsed source at the Rutherford Appleton Laboratory. Since the alkali-loaded zeolites are air- and moisture-sensitive, the data were collected using the quartz reaction vessel as a sample holder. To eliminate the amorphous silica background, data were also obtained from an empty sample tube. These data were then smoothed, appropriately scaled, and subtracted from the zeolite diffraction patterns to produce an essentially flat background. Data were obtained for five alkali loaded samples ($u = 1$, 3, 5, 7, and 9) together with the dehydrated host zeolite.

The structures were refined by the Rietveld method using the program TF14LS based on the Cambridge Crystallographic Subroutine Library.[14,15] Neutron scattering lengths of 0.367, 0.41534, 0.3449, and 0.5803 (all $\times 10^{-12}$ cm) were assigned to K, Si, Al, and O, respectively.[16] The structure was refined assuming the hexagonal space group *P*6/*mmm* (no systematic absences) as reported in previous studies of zeolite L.[17−19] The starting model for each refinement was that of Newsam.[18] In the first instance the positions of the framework atoms were refined before the introduction of any of the alkali cations. Although different silicon and aluminum occupancies have been reported for the two tetrahedral sites,[19] in view of the similarity in scattering lengths the Si to Al ratio was fixed at the theoretical value of 3.0 for both sites throughout the analyses. Initially only the potassium sites K1, K2, and K3 were considered, as these have been reported to contain essentially all of the potassium ions K_9-L and K_1/K_9-L. For the more heavily loaded samples, further potential potassium coordination sites were examined. These potassium sites were located using difference Fourier methods with subsequent refinement. Isotropic temperature factors were assigned to all atoms.

ESR Measurements. A portion of each of the samples prepared was sealed in the Spectrosil sidearm of the reaction tube so that ESR (and microwave cavity perturbation) measurements could be made without exposing the product to the atmosphere. The ESR spectra were recorded on a Bruker ESP 300 spectrometer operating at X-band frequencies (ca. 9 GHz) with 100 kHz field modulation. The microwave frequency was measured with a Hewlett-Packard 5350B frequency counter to an accuracy of ±1 kHz, and the magnetic field with a Bruker ER 035M NMR gaussmeter to better than ±0.1 G. To access temperatures down to 4 K, an Oxford Instruments ESR 900 continuous flow cryostat was used. These measurements were quantified through direct comparison of the signal intensity (obtained through double integration of the familiar first derivative ESR spectrum) with that of a $CuSO_4 \cdot 5H_2O$ standard in a dual-mode cavity. This procedure is estimated to yield values accurate to within ±20% of the absolute spin concentration.

Microwave Measurements of Electrical Conductivity. Measuring the electrical conductivity of air- and moisture-sensitive microcrystalline powders presents a formidable experimental challenge. In response to the intrinsic problems involved in such a measurement, we have developed a microwave cavity perturbation technique to measure the electrical conductivity σ of our powder samples without the need for sample contacts.[2,20,21] Similar techniques have been successful for evaluating the conductivity of powders in other systems.[22,23] At these high frequencies (3 GHz), the effects of powder intergrain contacts are negligible, and the microwave method probes the intragrain conductivity.

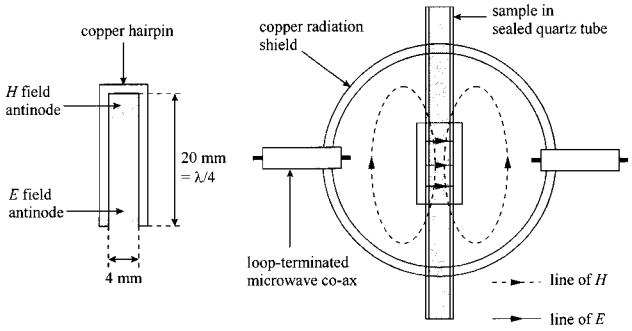

Figure 1. Schematic diagram of the 3 GHz copper hairpin resonator.

Figure 1 is a schematic diagram of the 3 GHz quarterwave copper hairpin used as the host cavity for the microwave conductivity measurements. This hairpin cavity has an unloaded quality factor Q of 2000 at room temperature, increasing to 4500 below 20 K (Q is defined as $Q = f_0/f_B$, where f_B is the resonant bandwidth at half power and f_0 is the resonant frequency). These Q factors are large for such a small cavity volume (≈0.8 cm^3), resulting in a very sensitive measurement of the zeolite response owing to the large sample filling factor in the cavity. Microwaves are coupled in to and out of the cavity using loop-terminated coaxial transmission lines, and the transmitted microwave power is measured as a function of frequency using a HP8720A vector network analyzer with computer control. The cavity is mounted in a Leybold closed-cycle cryocooler, allowing all measurements to be performed as a function of temperature in the range 10−295 K. The samples (see Figure 1) can be placed either at the antinode of the electric field E (at the open end of the hairpin, where the magnetic field is approximately zero) or at the antinode of the magnetic field H (at the closed end of the hairpin, where the electric field is approximately zero). Both fields are almost uniform at these end positions and measurements are presented for samples placed in each.

The increase in resonant bandwidth Δf_B associated with the insertion of a sample into the cavity is measured relative to the cavity containing an empty quartz tube. The microwave loss of the quartz tube is small compared to that of the zeolite samples, and its walls are thin enough not to cause significant alteration of the microwave electric field in its vicinity. In both of the sample positions, Δf_B is approximately proportional to the electrical conductivity of the sample (we will qualify this statement below). The implicit assumption here is that the radii of the grains of the powder are much less than the microwave skin depth of the fields within the grains, leading to complete penetration of either field into the sample. This assumption is valid for our zeolite powders, as is confirmed through ESR measurements, and as we shall see, by the relatively low conductivities measured for these compounds.

Results and Discussion

Structure. For each of the samples studied, least squares refinement of the framework atom positions together with those of K1, K2, and K3 (see Figure 2), converged smoothly to final values close to those previously reported for dehydrated potassium zeolite L.[18] In the case of dehydrated K_9-L and K_1/K_9-L all the potassium in the structure was accommodated in these three sites, as was reported in our previous study.[12] Complete occupancy of these sites leads to a total of 11 potassium ions per unit cell (equivalent to $u = 2$). This means that in the case of the more heavily loaded materials ($u \geq 3$), additional potassium coordination sites are required to account

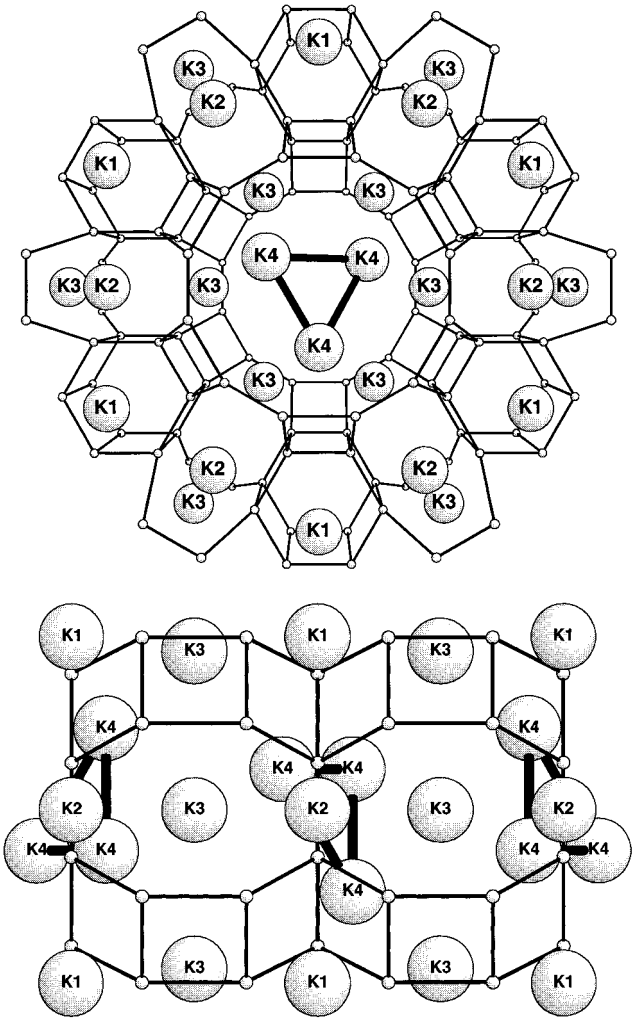

Figure 2. Representation of the structure of K_5/K_9-L showing the four different potassium sites: (a, top) viewed along the *c* direction (parallel to the one-dimensional channels); (b, bottom) viewed perpendicular to the *c* direction.

for all the added metal. A series of difference Fourier sections through the structure revealed additional scattering density in the large channels at around (0.08, 0.16, 0.38). Incorporation of this new potassium site (K4) into the structural model led to a significant improvement in the fit to the data and the refinements converged to the final values shown in Table 1. A representative profile fit is shown in Figure 3. This site, with multiplicity 12, is made up of two rings of six potassiums on either side of the 12-ring constrictions that divide the one-dimensional channels of zeolite L into segments. Examination of the potassium−potassium distances for this site in K_5/K_9-L (Table 2) imposes a limit of 3 ions/cell, a triangle made up of two potassiums in one ring of 6 and one potassium in the other ring, as shown in Figure 2.

A particularly noteworthy feature of the structures of this series of compounds is the evolution of the cell constants as a function of added potassium. The *a* lattice parameter, perpendicular to the 12-ring channels, shows a steady contraction with increasing potassium content. By contrast the *c* parameter, parallel to the channels, is essentially unchanged as far as $u = 3$ but expands for $u \geq 5$. The cell dimensions for the most heavily loaded samples correspond quite closely to previously reported values for hydrated K_9-L, suggesting that alkali metal inclusion may have a similar effect to hydration in reducing the electric fields associated with the imperfect coordination of potassium. Unfortunately, in the case of K_7/K_9-L and K_9/K_9-L, the detection of further stable potassium sites has proven difficult, and satisfactory refinement of the structures of these compounds has not yet been achieved. In K_9/K_9-L an observed deterioration in the crystallinity of the sample is a contributory factor to the problems experienced, but this is not the case for K_7/K_9-L. It may be that the extra potassium over and above the concentration $u = 5$, whose presence in these compounds is indicated by the continuing change in lattice parameters, is present in ill-defined "atomic" sites not bound to the zeolite framework.

A large body of previous work on alkali-metal-loaded zeolites supports the view that the reaction of alkali metals with dehydrated zeolites may be regarded as a dissolution process analogous to the dissolution of these same metals in polar solvents such as liquid ammonia.[2,3,11,24] In both cases the ionization of the metal atoms is central to the process. The crystallographic results reported here lend support to this picture. In K_5/K_9-L, for example, it is quite clear that all 14 potassiums per unit cell are located in sites, bonded to the oxygens of the aluminosilicate framework, that may be regarded as *primarily ionic* in nature. The major challenge in the study of alkali-metal-loaded zeolites is to establish the location of the resulting "excess electrons" released in the ionization process,[3] which are responsible for the electronic, magnetic and optical properties of interest in these compounds.

If the excess electrons were distributed evenly over all the potassium ions within the structure the average net charge per potassium, even in K_9/K_9-L, would still be +0.5. An examination of the trends in K−O bond lengths, however, provides clear indications of a less than even distribution of charge among the potassium ions. Selected bond lengths are presented in Table 2. The five potassium ions in the K1 and K2 sites occupy the less open region of the structure and should be the least affected by the increasing electron population associated with metal loading. Indeed the bond lengths for K2 remain relatively unaffected by the increasing potassium content, but those for K1 do show a steady increase. This is slightly surprising as the K1 sites are located at the center of each cancrinite cage in zeolite L, apparently rather more isolated than the K2 sites. The observed increase in bond length therefore could be evidence that the excess electrons are not confined to the large channels but penetrate the whole of the structure, but might also simply reflect changes in the geometry of the framework, in particular the contraction of the one-dimensional channels. The K3 site (6j) appears to accept a significant amount of electron density, gradually moving out into the channels as it does so. Examination of the dimensions of the 12-ring channels at their narrowest point ($z = 0.5$), as measured by the distance across the channel between equivalent oxygens (O1 or O2), reveals a pronounced contraction with increasing potassium content: the O1−O1 separation drops from 10.16 Å for dehydrated potassium zeolite L to 10.01 Å for K_5/K_9-L, while the O2−O2 distance contracts from 10.61 to 10.42 Å. This contraction of the 12-ring, even when each ring has as many as three K4 sites occupied in close proximity to one another, and the imperfect coordination of the K4 site itself, are strong indications of excess electron density on that site.

ESR. The room-temperature ESR spectra of K_u/K_9-L are shown in Figure 4. In all cases the spectrum consisted of a single main line, approximately lorenztian in shape. Parameters obtained from these spectra are given in Table 3. The room-temperature line width was found to drop from 20.9 G for $u = 1$ to 14.3 G for $u = 4$ before rising again to 48.6 G for $u = 9$. A secondary feature at higher field was also present in the ESR spectrum for $u \leq 3$. The temperature dependence of the

TABLE 1: Structural Parameters for K_u/K_9-L ($u = 0$, 1, 3, and 5)

	Wyckoff symbol			K_0/K_9-L	K_1/K_9-L	K_3/K_9-L	K_5/K_9-L
a/Å				18.4830 (6)	18.4498 (3)	18.3893 (3)	18.3628 (4)
c/Å				7.4938 (4)	7.4851 (2)	7.4828 (2)	7.5170 (3)
Si1/Al1	12q		*x*	0.0921 (6)	0.0919 (4)	0.0922 (4)	0.0914 (5)
			y	0.3546 (6)	0.3552 (4)	0.3561 (4)	0.3544 (5)
			B_{iso}	2.0 (2)	1.13 (11)	1.33 (12)	1.8 (2)
Si2/Al2	24r		*x*	0.1666 (5)	0.1681 (3)	0.1677 (3)	0.1675 (4)
			y	0.4990 (4)	0.4995 (3)	0.4991 (3)	0.4994 (4)
			z	0.2110 (7)	0.2121 (5)	0.2113 (5)	0.2115 (6)
			B_{iso}	0.90 (9)	0.57 (5)	0.77 (6)	1.01 (7)
O1	6k		*x*	0.2749 (5)	0.2740 (3)	0.2729 (4)	0.2726 (4)
			B_{iso}	1.23 (14)	0.89 (8)	1.13 (9)	1.05 (10)
O2	6m		*x*	0.1657 (3)	0.1655 (2)	0.1645 (2)	0.1638 (3)
			y	0.3313 (6)	0.3309 (4)	0.3290 (4)	0.3276 (5)
			B_{iso}	2.3 (2)	1.61 (11)	1.89 (12)	1.87 (15)
O3	12o		*x*	0.2653 (2)	0.2652 (1)	0.2647 (1)	0.2646 (2)
			y	0.5307 (4)	0.5303 (3)	0.5294 (3)	0.5293 (3)
			z	0.2576 (9)	0.2566 (7)	0.2525 (8)	0.2489 (9)
			B_{iso}	1.69 (12)	1.55 (7)	1.88 (9)	1.74 (9)
O4	24r		*x*	0.1004 (4)	0.1010 (2)	0.1011 (3)	0.1011 (3)
			y	0.4143 (4)	0.4150 (2)	0.4139 (3)	0.4134 (4)
			z	0.3225 (6)	0.3201 (4)	0.3180 (5)	0.3183 (6)
			B_{iso}	2.44 (12)	1.92 (7)	2.24 (8)	2.29 (10)
O5	12o		*x*	0.4261 (3)	0.4267 (2)	0.4266 (2)	0.4271 (2)
			y	0.8521 (5)	0.8534 (4)	0.8533 (4)	0.8543 (5)
			z	0.2720 (9)	0.2732 (6)	0.2735 (7)	0.2725 (8)
			B_{iso}	2.4 (2)	2.07 (10)	2.50 (11)	2.44 (14)
O6	12p		*x*	0.1457 (6)	0.1468 (3)	0.1462 (3)	0.1446 (4)
			y	0.4779 (4)	0.4776 (3)	0.4776 (3)	0.4759 (3)
			B_{iso}	1.70 (11)	1.57 (8)	1.71 (8)	1.85 (11)
K1	2d		B_{iso}	2.0 (5)	0.9 (3)	0.5 (3)	0.9 (4)
K2	3g		B_{iso}	3.5 (6)	3.5 (4)	3.5 (4)	3.8 (5)
K3	6j		*x*	0.3156 (14)	0.3136 (11)	0.3117 (11)	0.3057 (12)
			B_{iso}	2.5 (7)	5.6 (8)	4.0 (6)	5.8 (5)
		occupancy		0.73 (7)	0.93 (6)	0.86 (6)	1
K4	12o		*x*			0.082 (2)	0.079 (2)
			y			0.163 (3)	0.159 (4)
			z			0.349 (5)	0.386 (9)
			B_{iso}			0.0 (9)	4.1 (20)
		occupancy				0.13 (2)	0.22 (5)

R Factors (%)

K_0/K_9-L	$R_{wP} = 2.9$	$R_E = 2.8$	$R_I = 7.0$
K_1/K_9-L	$R_{wP} = 4.1$	$R_E = 2.8$	$R_I = 6.6$
K_3/K_9-L	$R_{wP} = 4.0$	$R_E = 2.8$	$R_I = 6.4$
K_5/K_9-L	$R_{wP} = 3.3$	$R_E = 2.5$	$R_I = 6.4$

$$R_{wP} = \left[\frac{\sum_i w_i |y_i(\text{obs}) - y_i(\text{calc})|^2}{\sum_i w_i y_i^2(\text{obs})}\right]^{1/2} \qquad R_E = \left[\frac{N - P + C}{\sum_i w_i y_i^2(\text{obs})}\right]^{1/2}$$

$$R_I = \left[\frac{\sum_k |I_k(\text{obs}) - (1/c) I_k(\text{calc})|}{\sum_k I_k(\text{obs})}\right]$$

[a] *N*, *P*, and *C* are the number of observations, parameters, and constraints respectively.

recorded ESR spectra was followed down to 4 K. The variation in the ESR line width for a number of samples can be seen in Figure 5. It is clear that the observed trends in room-temperature line width reflect differences in the temperature dependence of the line width. For $u < 5$ the line width varies only slightly with temperature, tending to decrease with increasing temperature, which suggests that the line width is governed by a motional averaging process.[2] For $u \geq 5$, however, the measured line width increases strongly with temperature, and the strength of this dependence increases with increasing metal content. Interestingly, these observations closely parallel measurements of the conductivity of the samples (see below), indicating a degree of correlation between the electron-spin and electron-transport behavior of these compounds.

The paramagnetic susceptibilities of the samples (expressed as spin concentrations in Table 3) are very small. In column 5 of Table 3 the intensities of the observed ESR signals are expressed as a percentage of that expected for *u* moles of

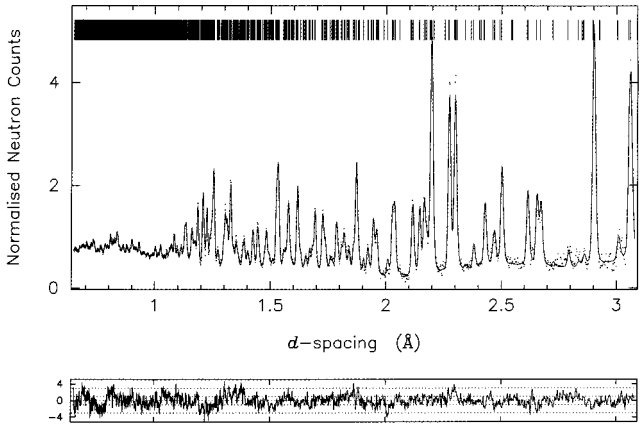

Figure 3. Observed and calculated neutron diffraction patterns for K_3/K_9-L.

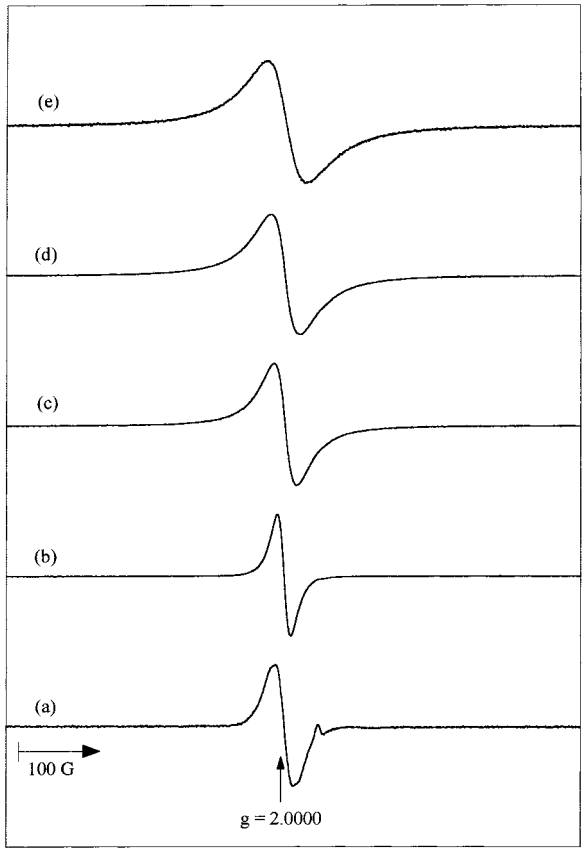

Figure 4. Room-temperature ESR spectra of K_u/K_9-L: (a) $u = 1$, (b) 3, (c) 5, (d) 7, and (e) 9.

TABLE 2: Selected Bond Lengths in K_u/K_9-L

	K_0/K_9-L	K_1/K_9-L	K_3/K_9-L	K_5/K_9-L
K1−O3	2.836(10)	2.840(8)	2.865(8)	2.887(9)
K1−O5	3.425(13)	3.433(9)	3.421(10)	3.439(11)
K2−O4	3.266(12)	3.273(10)	3.280(10)	3.285(11)
K2−O5	2.918(13)	2.893(9)	2.885(10)	2.881(11)
K3−O4	3.04(3)	3.03(2)	3.03(2)	3.07(2)
K3−O6	2.86(3)	2.87(2)	2.89(2)	2.92(2)
K4−O1			3.26(8)	3.21(11)
K4−O2			2.88(8)	2.83(11)
K3−K4			4.54(9)	4.66(12)
K4−K4			4.50(16)	4.37(22)
K4−K4			5.03(16)	4.70(22)

noninteracting spins. Observed spin fractions of only 1−4% indicate that the vast majority of the electrons introduced to the zeolite through the ionization of incoming potassium atoms are invisible to ESR. Again the jump from ~ 1% for $u < 5$ to ~3% for $u \geq 5$ would seem to indicate a relatively abrupt change in the measured properties of the samples at this composition. Much higher observed spin fractions have been reported[24,25] in zeolites containing the sodalite cage structural unit, which is known to be the site of stable paramagnetic clusters such as Na_4^{3+} and K_4^{3+}.[24,26] In many cases the presence of such species, which consist of a single unpaired electron delocalized over four cations, is confirmed by the observation of a characteristic ESR hyperfine splitting pattern, but in no case at any temperature was any evidence of hyperfine splitting detected in K_u/K_9-L.

TABLE 3: ESR Parameters for K_u/K_9-L

sample	g (±0.0002)	ΔH_{pp} (±0.2 G)	RT spin susceptibility (spins/cm^3)	obsd spin fraction (%)
K_1/K_9-L	1.9985[a]	20.9	4.5×10^{18}	1.0
K_2/K_9-L	1.9986[a]	18.0	1.2×10^{19}	1.3
K_3/K_9-L	1.9987	16.3	1.9×10^{19}	1.4
K_4/K_9-L	1.9986	14.3	2.2×10^{19}	1.2
K_5/K_9-L	1.9984	28.1	7.4×10^{19}	3.3
K_7/K_9-L	1.9982	35.5	8.5×10^{19}	2.7
K_9/K_9-L	1.9973	48.6	1.4×10^{20}	3.4

[a] A secondary feature was also observed at $g = 1.9734 \pm 0.0002$.

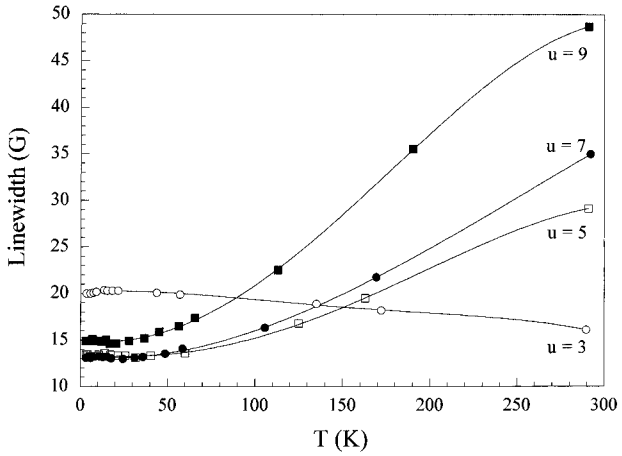

Figure 5. ESR line width for K_u/K_9-L as a function of temperature.

Conductivity. We first discuss measurements of the resonant bandwidth and resonant frequency for samples placed in the microwave electric field. Measurements of the transmitted resonant response as a function of frequency at room temperature are shown in Figure 6. Resonant bandwidths (and hence sample conductivities) increase with increasing potassium content, with a pronounced increase in bandwidth at $u = 5$, associated with a large rise in sample conductivity. The decrease in frequency measured for samples with increasing potassium content is associated with an increased relative permittivity.

To derive the conductivity from these data, we assume that each powder grain is an isotropic sphere with a complex relative permittivity $\epsilon = \epsilon' - i\epsilon''$ (where $\epsilon'' = \sigma/\omega_0\epsilon_0$, and $\omega_0 = 2\pi f_0$ is the angular resonant frequency); the issue of anisotropic grains is discussed below. Suppose that the grains are loosely packed, occupying a volume fraction β (typically 0.35) of the space inside the quartz tube. In the quasi-static case, the local field corrections of the polarized spheres can be included in the analysis, giving an effective complex relative permittivity of the powder sample of

$$\epsilon_{\text{eff}} \approx 1 + \frac{3\beta(\epsilon - 1)}{(1 - \beta)\epsilon + (2 + \epsilon)}$$

We have ignored the depolarizing effects of the quartz tube

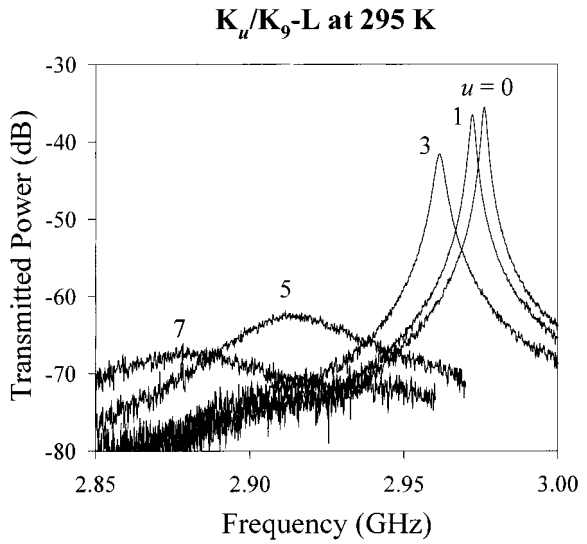

Figure 6. Transmitted resonant response of the 3 GHz resonator, containing K_u/K_9-L samples placed at the microwave electric field antinode (see text), as a function of frequency at room temperature.

holding the sample since its walls are very thin. Standard microwave cavity perturbation theory[27] can now be used to express the resonant frequency shift and bandwidth change associated with the sample when placed in the electric field region (Figure 1) in terms of ϵ, giving

$$-\frac{\Delta f_0^{\text{elec}}}{f_0} \approx \frac{3}{2}\alpha\beta\frac{(\epsilon'-1)(\epsilon'+2-\beta[\epsilon'-1])+(1-\beta)\epsilon''^2}{(\epsilon'+2-\beta[\epsilon'-1])^2+(1-\beta)^2\epsilon''^2} \quad (1)$$

$$\frac{\Delta f_B^{\text{elec}}}{f_0} \approx 9\alpha\beta\frac{\epsilon''^2}{(\epsilon'+2-\beta[\epsilon'-1])^2+(1-\beta)^2\epsilon''^2} \quad (2)$$

where Δf_0^{elec} and Δf_B^{elec} are the changes in resonant frequency and bandwidth, respectively, when a sample is placed in the electric field antinode of the cavity; both are measured relative to the values obtained for an empty quartz tube placed at the same position. The energy filling factor α is

$$\alpha = \int_{\text{sample}} E_0^2\, dV / \int_{\text{cavity}} E_0^2\, dV$$

where E_0 is the magnitude of the unperturbed electric field within the cavity and the volume integrals are carried out within the regions indicated; for our hairpin cavity

$$\alpha \approx \frac{2V_{\text{sample}}}{V_{\text{cavity}}} \approx 0.24$$

Equations 1 and 2 can be solved simultaneously to find ϵ' and $\epsilon'' = \sigma/\omega_0\epsilon_0$ from the experimental data. When $\epsilon'' \ll \epsilon'$, we see from eq 2 that $\Delta f_B^{\text{elec}} \propto \epsilon'' \propto \sigma$, as we assumed earlier. A significant systematic error is introduced here owing to uncertainties in β. The estimated error of $\pm 15\%$ in β gives rise to errors of around $\pm 30\%$ in the absolute values of ϵ; however, for a set of measurements on a given sample this error is fixed and much smaller changes in the conductivity occurring as a function of temperature are reliably detected. In Figure 7 we plot the temperature dependence of the conductivity extracted from the electric field data. In Figure 8a,b we plot the relative permittivity ϵ' and conductivity σ respectively, as a function of potassium content at both 15 and 280 K. We find that ϵ' does not vary significantly with temperature until we reach potassium contents $u \geq 5$; then ϵ' becomes temperature-dependent,

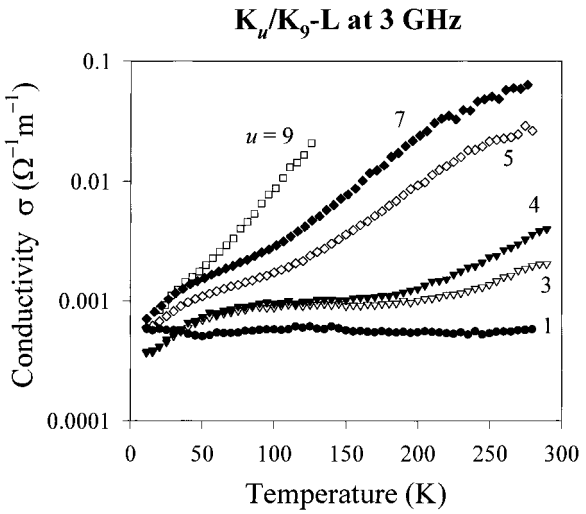

Figure 7. Conductivity of K_u/K_9-L as a function of temperature measured at the electric field antinode.

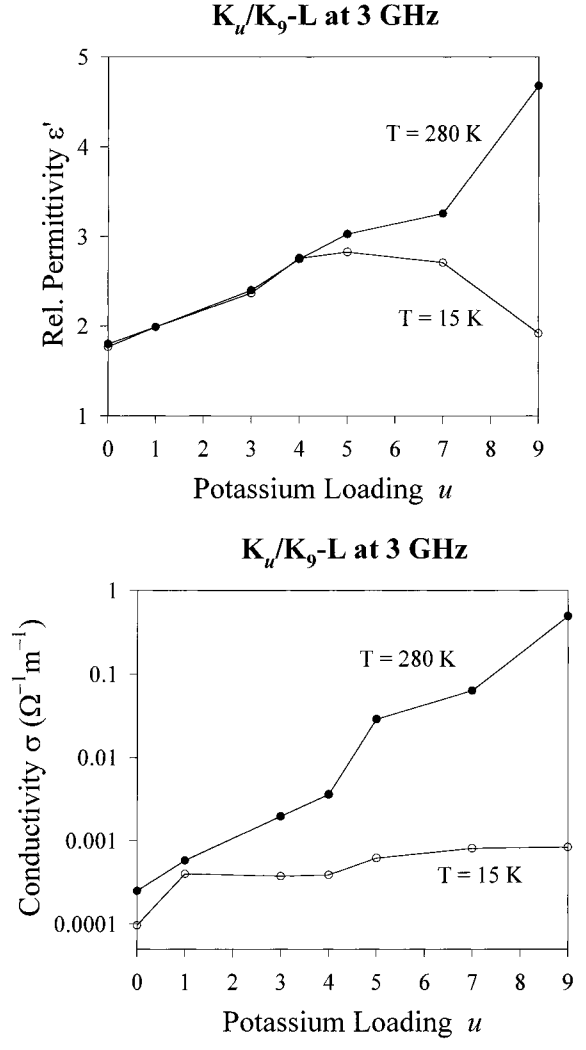

Figure 8. (a, top) Relative permittivity and (b, bottom) conductivity of K_u/K_9-L at 15 and 280 K.

decreasing with increasing u at low temperature, while increasing with increasing u at high temperature. The origin of this behavior is unclear but may be linked to the sudden increase in electrical conductivity that occurs for $u \geq 5$. The conductivity at low temperature is approximately constant for all values of potassium content. At higher temperature, however, the room-temperature conductivity increases rapidly with potassium

content, with a marked jump when $u \geq 5$. Overall, the inclusion of potassium metal in potassium zeolite L results in an increase in the measured room-temperature conductivity of around 4 orders of magnitude. The highest values of conductivity achieved in this study are when $u = 9$ at room T, where $\sigma \approx 0.5\ \Omega^{-1}\ m^{-1}$. The corresponding microwave skin depth at 3 GHz is about 1.3 cm, which is considerably larger than the mean zeolite grain size (around 10 μm), confirming the validity of our initial assumption of complete microwave field penetration into the grains. In keeping with the relatively modest values of conductivity, none of the temperature dependences of Figures 7 and 8b are characteristic of metallic conduction, where we would expect the conductivity to decrease with increasing temperature. The observed behavior indicates a thermally activated conduction mechanism, though without a unique activation energy.

The data analysis above assumes an isotropic σ, but in the extreme anisotropic limit (which would be appropriate for metallic conduction along the zeolite channels) the effective conductivity produced by this analysis is simply $\sigma_{||}/3$, where $\sigma_{||}$ is the conductivity along the channels. The factor of $^1/_3$ arises when averaging the power dissipated for a powder sample whose grains are oriented randomly relative to the direction of the applied electric field. To see if this correction factor is appropriate and to address further the issue of sample anisotropy, we performed the same measurements on the same samples placed in the microwave magnetic field.

The increases of the resonant bandwidths for samples placed in the magnetic field are due to the eddy current losses in each grain of the powder and a different analysis is necessary. To extract a precise value for σ, we need to know in detail the grain size distribution of the powder, otherwise there are considerable systematic errors in the values of conductivity extracted.[22] Consequently, we keep the analysis in this configuration semiquantitative. Faraday's law tells us that the microwave magnetic field will induce an electric field of magnitude E within the powder grains, and so the contribution of the sample to the resonant bandwidth Δf_B^{mag} (which is proportional to the power dissipated in the sample) is

$$\Delta f_B^{mag} \propto \sigma \int_{sample} E^2\, dV \propto \sigma$$

Any eddy currents induced along the channels in zeolite L must have a return path perpendicular to the channels. In the extreme anisotropic limit, the interchannel conductivity $\sigma_\perp$ is much lower than the intrachannel conductivity $\sigma_{||}$, and the contribution to the bandwidth is therefore proportional to this small, interchannel conductivity,[23] i.e.

$$\Delta f_B^{mag} \propto \sigma_\perp \qquad (3)$$

Without detailed knowledge of the powder grain size distributions, we cannot evaluate the appropriate scaling factor in eq 3.

Results for $\Delta f_B^{mag}(T) = A\sigma_\perp(T)$, where A is the unknown scaling factor, are plotted in Figure 9. Again there is a large jump in conductivity at $u = 5$, similar to the results in the electric field, associated with the increase of $\sigma_\perp$ with potassium content. The temperature dependences of both $\sigma_\perp$ and $\sigma_{||}$ (from Figure 7) show very similar, thermally activated behavior. This is illustrated further in Figure 10, where we compare the two sets of data for $u = 7$ (we have arbitrarily scaled the magnetic field data to illustrate the correspondence between the two sets of data). The data differ significantly only below 100 K, and this is likely to be due to the systematic errors introduced in this

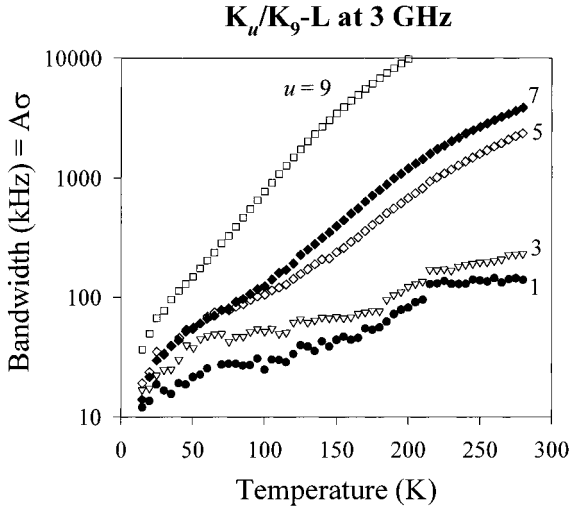

Figure 9. Resonant bandwidth of K_u/K_9-L as a function of temperature measured at the magnetic field antinode. (*A* is an unknown scaling factor.)

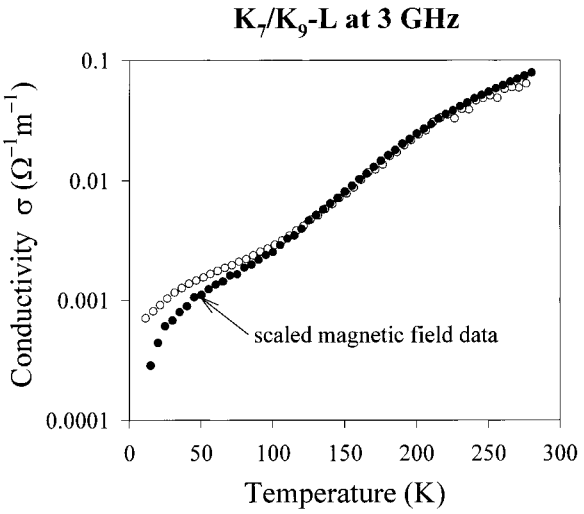

Figure 10. Comparison of the conductivity of K_7/K_9-L (see text) measured at the electric field (open circles) and magnetic field (filled circles) antinodes.

range when subtracting the residual bandwidth of the cavity and quartz tube from the zeolite data. We conclude from these measurements that if any anisotropy is present, it is clearly not large in these samples. Consequently, we do not distinguish between $\sigma_\perp$ and $\sigma_{||}$ in any of the figures presented. This conclusion is in agreement with the findings of Kelly,[4] who has developed a model for the electronic properties of this system. He predicts that strong interchannel interactions facilitated by the relatively small interchannel separation in zeolite L should limit any anisotropy in the measured conductivity to around a factor of 2, almost certainly too low to be detected by our current measurements.

A Role for K_3^{p+}? From the results presented above it is clear that the inclusion of potassium metal in potassium zeolite L results in a substantial increase in the measured room-temperature conductivity, by around 4 orders of magnitude. It is also apparent that much of this enhanced conductivity is present only in samples whose potassium loading approaches or exceeds the composition $u = 5$. The importance of this composition as a threshold value is evident in all three types of measurements reported in this paper. In crystallographic terms $u = 5$ is the composition at which the conventional potassium sites (K1, K2, and K3) are completely filled, leaving three potassiums (the postulated maximum) in K4 sites forming a

trimer at each neck in the one-dimensional channels (see Figure 2). We interpret the three K4 cations located at each 12-ring constriction in the one-dimensional channels in K_5/K_9-L as a K_3^{p+} cluster. The K4−K4 distances (see Table 2) are considerably shorter in K_5/K_9-L than in K_3/K_9-L. The latter contains on average only one K4 potassium at each constriction and the distances quoted in Table 2 for this compound may well be virtual. Nevertheless, the fact that the equivalent distances in K_5/K_9-L—in this case certainly not virtual—are so much shorter, is strong evidence for bonding between the K4 ions. The contraction in the 12-rings which accompanies occupation of the K4 site is also most plausibly explained as evidence of bonding in such a cluster. As the K4 cations remain strongly bound to the framework oxygens it is likely that the unit retains an overall positive charge with $p = 1$ or 2. The overall weakness of the paramagnetism in these compounds, with only 1−4% of the excess electron spins detected (Table 3), would appear to point to the diamagnetic K_3^+ species, but the presence of at least some K_3^{2+} units cannot be ruled out.

By comparison of diffuse-reflectance spectra of UV-irradiated potassium L with those from similarly treated potassium X, Liu and Thomas[28] inferred the presence of K_3^{2+} clusters, which they suggested consisted of a triangle of either two K2 ions and one K3 or one K2 and two K3. ESR provides no direct evidence in the form of hyperfine splitting for the presence such clusters in K_u/K_9-L, but this could easily be lost through spin exchange interactions.[2] As discussed above, however, there is no evidence from the crystal structures for excess electron density on the K2 cations, and although there is evidence for excess electrons associated with the K3 site, this has the effect of pulling the K3 cations into the channels and thus increasing the already relatively long K2−K3 bond distance (∼5.2 Å). This movement is part of a general contraction in the one-dimensional channels with increasing potassium loading, which occurs although the extra potassium is located in these channels and is a strong indication that the excess electrons are located here rather than in clusters involving the K2 site.

In the K_u/K_9-L system, the K4 site first becomes occupied at potassium loadings above $u = 2$, the point at which the K3 site is filled. At this point the one-dimensional channels contain only K3 potassiums arranged in hexagonal rings perpendicular to the channel direction, which are separated from each other along the channels by a distance equal to the *c* parameter (∼7.5 Å). A further increase in potassium content results in the progressive occupation of the K4 sites. As discussed above, these are located on either side of the 12-ring constrictions, which occur midway between K3 rings, thus effectively halving the distance between potassium cations along the channel direction. Clearly this could have a significant effect on the electrical conductivity of the samples. The most significant change in conductivity, however, occurs between $u = 4$ and $u = 5$, i.e., when the K4 site is more than two-thirds full, and when K_3^{p+} clusters must begin to form. It may well, therefore, be the K_3^{p+} clusters which are responsible for the observed jump in conductivity. It is possible that a K_3^{2+}/K_3^+ redox hopping process is important in mediating the transfer of electrons through the constrictions in the one-dimensional channels and that this is the key step in the thermally activated conduction process. Certainly, this proposal would explain the large increase in measured conductivity at around $u = 5$, the composition at which there is enough potassium for one K_3^{p+} cluster at each constriction.

Although there is no evidence for significant anisotropy in the conductivity measurements discussed above, the secondary feature observed in the ESR spectrum of some samples has previously been interpreted as a sign of anisotropy.[12] Significantly this is observed only at low potassium loadings ($u \leq 3$), implying that anisotropy decreases with increasing *u*. In this respect it is important to note that the K4 sites are closer to K1 and K2 than the K3 sites are and that the K_3^{p+} clusters are therefore well placed to interact with ions in the less open part of the structure, which may in turn play a part in mediating interchannel interactions.

Conclusions

The incorporation of extra potassium into dehydrated potassium zeolite L resulted in an increase in the room-temperature conductivity by around a factor of 10 000, to a value similar to that observed in lightly doped semiconductors such as silicon, but somewhat short of values anticipated for metals such as copper. In making these comparisons, however, it must be remembered that the zeolite-based systems, even at the highest metal loadings, have low excess electron (potential carrier) densities, particularly when compared to the highly conducting elemental metals. The strong temperature dependence of the measured conductivities is characteristic of a thermally activated conduction mechanism, albeit without a unique activation energy. As predicted by Kelly,[4] we found no evidence of anisotropy in the conductivity of any of the compounds measured, presumably as a result of strong interchannel interactions. In K_5/K_9-L we report the observation of a new K_3^{p+} cluster located within the one-dimensional channels of zeolite L. ESR and conductivity measurements show that the presence of this species has an important effect on the electronic properties and in particular on the conductivity of this compound.

Acknowledgment. We would like to thank the EPSRC for support and provision of neutron beam facilities. We thank the Royal Society for the award of a University Research Fellowship (P.A.A.) and a Leverhulme Senior Research Fellowship (P.P.E.).

References and Notes

(1) Anderson, P. A.; Bell, R. G.; Catlow, C. R. A.; Chang, F. L.; Dent, A. J.; Edwards, P. P.; Gameson, I.; Hussain, I.; Porch, A.; Thomas, J. M. *Chem. Mater.* **1996**, *8*, 2114.

(2) Anderson, P. A.; Edwards, P. P. *J. Am. Chem. Soc.* **1992**, *114*, 10608.

(3) Edwards, P. P.; Anderson, P. A.; Thomas, J. M. *Acc. Chem. Res.* **1996**, *29*, 23.

(4) Kelly, M. J. *J. Phys. Condensed Matter* **1995**, *7*, 5507.

(5) Rabo, J. A.; Angell, C. L.; Kasai; P. H.; Schomaker, V. *Discuss. Faraday Soc.* **1966**, *41*, 328.

(6) Edwards, P. P.; Harrison, M. R.; Klinowski, J.; Ramdas, S.; Thomas, J. M.; Johnson; D. C.; Page, C. J. *J. Chem. Soc., Chem. Commun.* **1984**, 982.

(7) Harrison, M. R.; Edwards, P. P.; Klinowski, J.; Thomas, J. M.; Johnson, D. C.; Page, C. J. *J. Solid State Chem.* **1984**, *54*, 330.

(8) Anderson, P. A.; Singer, R. J.; Edwards, P. P. *J. Chem. Soc., Chem. Commun.* **1991**, 914.

(9) Anderson, P. A.; Edwards, P. P. *J. Chem. Soc., Chem. Commun.* **1991**, 915.

(10) Anderson, P. A.; Barr, D.; Edwards, P. P. *Angew. Chem.* **1991**, *103*, 1511; *Angew. Chem., Int. Ed. Engl.* **1991**, *30*, 1501.

(11) Edwards, P. P.; Woodall, L. J.; Anderson, P. A.; Armstrong, A. R.; Slaski, M. *Chem. Soc. Rev.* **1993**, *22*, 305.

(12) Anderson, P. A.; Armstrong, A. R.; Edwards, P. P. *Angew. Chem* **1994**, *106*, 669; *Angew. Chem., Int. Ed. Engl.* **1994**, *33*, 641.

(13) Kelly, M. J. *Int. J. Electron.* **1993**, *75*, 27.

(14) Matthewman, J. C.; Thompson, P.; Brown, P. J. *J. Appl. Crystallogr.* **1982**, *15*, 167.

(15) Brown, P. J.; Matthewman, J. C. Rutherford Appleton Laboratory Report RAL-87-010, 1987.

(16) Sears, V. F. *Neutron News* No. **1992**, *3*, 26.

(17) Barrer, R. M.; Villiger, H. Z. *Kristallogr. Kristallgeom. Kristallphys. Kristallchem.* **1969**, *128*, 352.

(18) Newsam, J. M. *J. Phys. Chem.* **1989**, *93*, 7689.
(19) Newsam, J. M. *Mater. Res. Bull.* **1986**, *21*, 661.
(20) Anderson, P. A.; Woodall, L. J.; Porch, A.; Armstrong, A. R.; Hussain, I.; Edwards, P. P. *Mater. Res. Soc. Symp. Proc.* **1995**, *384*, 9.
(21) Edwards, P. P.; Anderson, P. A.; Woodall, L. J.; Porch, A.; Armstrong, A. R. *Mater. Sci. Eng. A* **1996**, *217/218*, 198.
(22) Waldram, J. R.; Porch, A.; Cheah, H. M. *Physica C* **1994**, *232*, 189.
(23) Liu, C. C.; Na, B. K.; Walters, A. B.; Vannice, M. A. *Catal. Lett.* **1994**, *26*, 9.
(24) Woodall, L. J.; Anderson, P. A.; Armstrong, A. R.; Edwards, P. P. *J. Chem. Soc., Dalton Trans.* **1996**, 719.
(25) Woodall, L. J.; Anderson, P. A.; Armstrong, A. R.; Edwards, P. P. *Mater. Res. Soc. Symp. Proc.* **1995**, *384*, 523.
(26) Armstrong, A. R.; Anderson, P. A.; Woodall, L. J.; Edwards, P. P. *J. Am. Chem. Soc.* **1995**, *117*, 9087.
(27) Staelin, D. H.; Morgenthaler, A. W.; Kong, J. A. *Electromagnetic Waves*; Prentice Hall: Upper Saddle River, NJ, 1994; p 375.
(28) Liu, X.; Thomas, J. K. *J. Chem. Soc., Faraday Trans.* **1995**, *91*, 759.